Controlled Release from Bilayer-Decorated Magnetoliposomes *via* Electromagnetic Heating

Yanjing Chen, Arijit Bose, and Geoffrey D. Bothun*

Department of Chemical Engineering, University of Rhode Island, 16 Greenhouse Road, Kingston, Rhode Island 02881

ABSTRACT Nanoscale assemblies that can be activated and controlled through external stimuli represent a next stage in multifunctional therapeutics. We report the formation, characterization, and release properties of bilayer-decorated magnetoliposomes (dMLs) that were prepared by embedding small hydrophobic SPIO nanoparticles at different lipid molecule to nanoparticle ratios within dipalmitoylphosphatidylcholine (DPPC) bilayers. The dML structure was examined by cryogenic transmission electron microscopy and differential scanning calorimetry, and release was examined by carboxyfluorescein leakage. Nanoparticle heating using alternating current electromagnetic fields (EMFs) operating at radio frequencies provided selective release of the encapsulated molecule at low nanoparticle concentrations and under physiologically acceptable EMF conditions. Without radio frequency heating, spontaneous leakage from the dMLs decreased with increasing nanoparticle loading, consistent with greater bilayer stability and a decrease in the effective dML surface area due to aggregation. With radio frequency heating, the initial rate and extent of leakage increased significantly as a function of nanoparticle loading and electromagnetic field strength. The mechanism of release is attributed to a combination of bilayer permeabilization and partial dML rupture.

KEYWORDS: magnetoliposome · SPIO nanoparticle · self-assembly · lipid bilayer · drug delivery

An emerging concept in liposome research is the design of hybrid liposomes containing functional nanoparticles as nanoscale therapeutics.[1−3] Liposomes, which consist of an ~5 nm thick lipid bilayer shell surrounding an aqueous core, can provide a means of dispersing and concentrating nanoparticles *via* encapsulation or binding, shielding them from biomolecular adsorption, and delivering them through established liposome targeting strategies. When loaded with drugs and nanoparticles, they resemble a classic liposome−drug formulation with additional functionality owing to the nanoparticles. This functionality could be related to imaging,[3−8] biosensing,[9] or heating through external activation using lasers[10−13] or alternating current electromagnetic fields (AC EMFs).[14−17]

A challenge to liposomal drug delivery is designing a liposome that is stable and long-circulating *in vivo* yet can be destabilized in a controlled fashion to facilitate drug release at the target site.[18] Drug release is controlled by diffusion through the lipid bilayer, which is greatest when the bilayer is disrupted or phase separated (*e.g.*, at the lipid main phase transition or melting temperature). Liposomes can lose a significant portion of their drug cargo in circulation, and upon arriving at a target site, the ability to control release can be poor. Decorating liposomes with bound nanoparticles and then supplying selective and local heating to the bilayer could, in principle, be used to control liposomal drug delivery.

Magnetoliposomes (MLs) were the first multifunctional hybrid liposome/nanoparticle assembly and have received considerable attention since being introduced in 1988.[19] Common strategies to ML design include (i) adsorbing a lipid bilayer onto the surface of a "large" superparamagnetic iron oxide (SPIO) nanoparticle or (2) encapsulating many "small" SPIO nanoparticles within the aqueous liposome core.[2,4,14−17,20,21] Their multifunctionality stems from the nature of SPIO nanoparticles. Magnets can be used to guide MLs *in vivo*, and the nanoparticles enhance contrast for MRI imaging.[22−25] MLs can also be heated in AC EMFs operating at radio frequency (RF) to provide localized hyperthermia treatment if delivered to a target site. RF heating is achieved *via* magnetic losses of the SPIO nanoparticles through Néel and Brown relaxation.[26] The advantage of RF energy is that it can easily penetrate the body and is non-invasive for up to 1 h if the product, Hf, where H is the field amplitude (current × number of coils per length) and f is the frequency, is below 4.85×10^5 kA m^{-1} s^{-1}.[27]

To improve on the sensitivity and responsiveness of MLs, we have formed

*Address correspondence to bothun@egr.uri.edu.

Received for review February 9, 2010 and accepted May 10, 2010.

Published online May 27, 2010.
10.1021/nn100274v

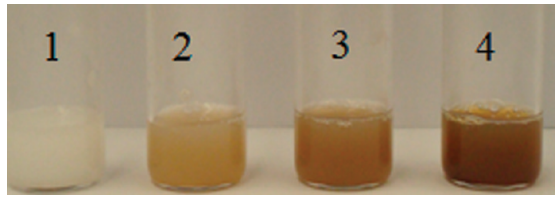

Figure 1. Digital images of (1) DPPC and dMLs prepared at *L/N* ratios of (2) 25000:1, (3) 10000:1, and (4) 5000:1. The lipid concentration was 10 mM.

bilayer-decorated MLs (dMLs) containing small hydrophobic SPIO nanoparticles, 5 nm maghemite (Fe_2O_3) capped with oleic acid (OA), embedded within lipid bilayers. We hypothesized that focused heating of embedded nanoparticles could be used to control and maximize leakage with minimal nanoparticle loading and EMF strengths. The embedment strategy employed is based on previous observations that hydrophobic C_{60} fullerene,[28,29] gold,[30,31] silver,[32,33] silicon,[34] and quantum dot[5−8,30] nanoparticles can be embedded within lipid bilayers without significantly compromising liposome structure. This approach compliments previous studies on embedding hydrophobic nanoparticles into polymersomes,[35,36] which are more stable than liposomes but do not offer the same level of biocompatibility. In this article, we report the formation of dMLs using dipalmitoylphosphatidylcholine (DPPC) as a model lipid at different nanoparticle loadings, expressed as the lipid molecule to nanoparticle ratio (*L/N*). The effect of loading on dML structure, lipid phase behavior, and liposomal release with and without RF heating is demonstrated.

RESULTS AND DISCUSSION

Sample Preparation. A detailed description of dML formation is provided in Methods. The dMLs were loaded with SPIO nanoparticles at *L/N* ratios of 25000:1, 10000:1, and 5000:1. These ratios corresponded to total Fe_2O_3 molar concentrations of 0.48, 1.20, and 2.40 mM, mass concentrations of 0.08, 0.19, and 0.38 mg/mL, and nanoparticle volume fractions within the bilayers of 0.002, 0.005, and 0.011, respectively (based on the molecular volume of DPPC at 50 °C[37]). Excess or unbound OA present in the as-received nanoparticle dispersions led to DPPC to OA mole ratios of 45.5, 18.2, and 9.1 with increased nanoparticle loading. Digital images of DPPC and dML samples are shown in Figure 1. With as-received dispersions, the dMLs exhibited the same settling behavior as DPPC liposomes at room temperature based on visual observation. Hence, nanoparticle embedding did not alter their relative stability.

Structural Characterization. Cryogenic transmission electron microscopy (cryo-TEM) was used to verify nanoparticle loading and its effect on dML structure (Figure 2). DPPC formed primarily unilamellar liposomes with an average diameter of 101 ± 22 nm (Figure 2A). Little change in liposome size, 102 ± 12 nm, was observed for dMLs prepared at a *L/N* of 25000:1 relative to DPPC. At higher nanoparticle loadings or lower *L/N* ratios, the dMLs were larger than DPPC liposomes and contained smaller liposomes encapsulated within larger liposomes (Figure 3B−D). The size of the dMLs increased with the *L/N* ratio from an average diameter of 156 ± 30 nm at 10000:1 to 198 ± 46 nm at 5000:1. Dark regions prevalent within the dMLs prepared at the two higher

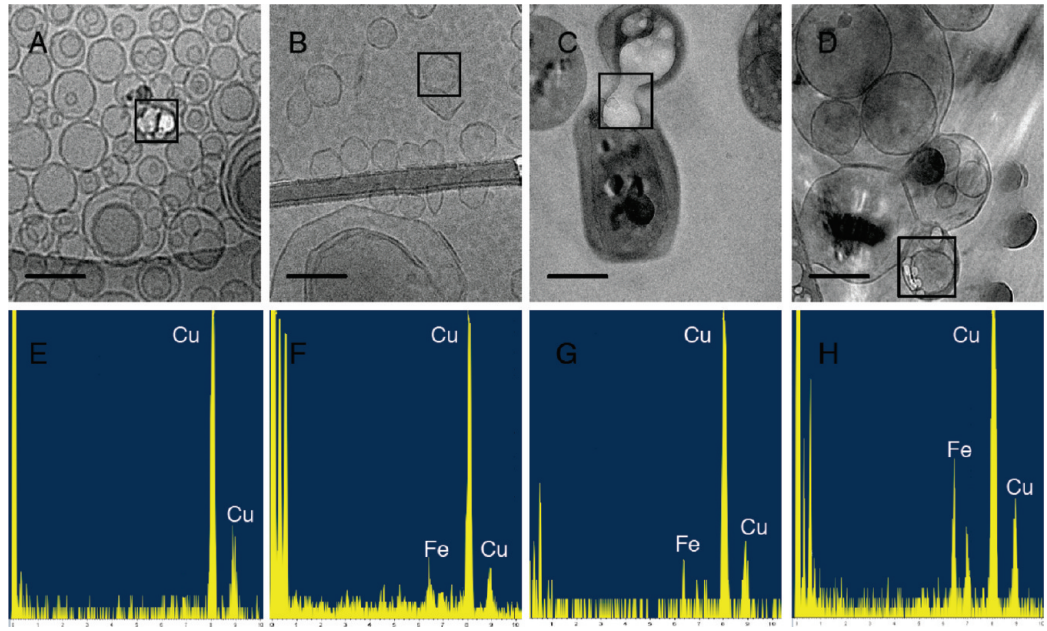

Figure 2. Cryo-TEM images and EDS maps of (A,E) DPPC liposomes and dMLs prepared at *L/N* ratios of (B,F) 25000:1, (C,G), 10000:1, and (D,H) 5000:1. The black scale bars are 200 nm. For imaging, the samples were incubated in the chamber at 25 °C under 100% humidity before vitrifying in liquid ethane. Iron (Fe) from the SPIO nanoparticles and copper (Cu) from the TEM grids are denoted in the EDS maps of the respective square regions.

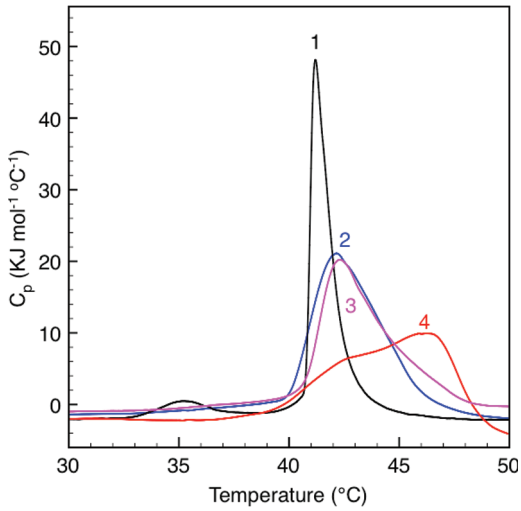

Figure 3. DSC thermographs of (1) DPPC and dMLs formed at *L*/*N* ratios of (2) 25000:1, (3) 10000:1, and (4) 5000:1. The samples were subjected to three consecutive heating/cooling cycles between 15 and 50 at 1 °C min^{-1}. The third heating scan is shown.

loadings depict SPIO nanoparticle aggregates associated with the bilayer. Neither SPIO nanoparticles nor nanoparticle aggregates were observed outside of the dMLs.

Nanoparticle loading was further verified by measuring elemental iron using energy-dispersive X-ray spectroscopy (EDS). It is important to note that the measurements were taken of sample regions where dMLs existed, and SPIO nanoparticle aggregates were not prevalent. Iron was not observed in DPPC liposomes (Figure 2E), while clear peaks were measured in each dML sample (Figure 2F−H). Nanoparticles were not detected outside of the dMLs based on random EDS mapping (results not shown). Hence, all SPIO nanoparticles appear to have existed within the liposomal bilayers as either individual nanoparticles or encapsulated aggregates.

Lipid Phase Behavior. Lipid phase behavior is sensitive to the presence of exogenous compounds or surfaces. Without embedded nanoparticles, DPPC exhibited a characteristic pretransition (T_p) at 35.2 °C and main transition at 41.2 °C (Figure 3). The pretransition describes the ordered gel ($L_{b'}$) to rippled gel ($P_{b'}$) phase transition, and the main transition or melting temperature describes the $P_{b'}$ to disordered fluid phase (L_a) transition. Two events were observed when SPIO nanoparticles were embedded; the pretransitions were suppressed and merged with lipid melting at higher temperatures, and the melting regions were broadened and also shifted to higher temperatures. These events were more pronounced with increasing nanoparticle loading. Deconvoluting the thermographs further indicated that the melting regions were composed of multiple overlapping peaks, which was clearly evident at the highest *L*/*N* ratio of 5000:1 ($R^2 \geq 0.997$; peakfit results not shown). At *L*/*N* ratios of 25000:1 and 10000:1, three overlapping peaks were resolved at 39.5, 42.2, 44.4 °C and 41.9, 42.7, and 44.4 °C, respectively. At a *L*/*N* ratio of 5000:1, peaks at 40.8, 42.7, 46.0, and 47.3 °C were resolved. Results were reproducible over four consecutive increasing and decreasing temperature scans with three different samples at a given *L*/*N* ratio (results not shown). These changes were not caused by the presence of excess oleic acid, which has been shown to decrease DPPC melting temperature.[38]

The first peak in the thermographs is attributed to higher temperature pretransitions and the remaining peaks to mixed DPPC/nanoparticle regions with increasing nanoparticle concentrations. Increases in melting temperature indicate that the nanoparticles preferred to mix with lipids in the gel phase rather than the fluid phase. The steric thickness of gel phase DPPC bilayers (5.2 nm at 20 °C[37]) is greater than that of fluid phase bilayers (4.7 nm at 50 °C[37]) and may have better accommodated the 5 nm SPIO nanoparticles. This phenomenon has been observed for transmembrane proteins with hydrophobic core lengths that better "match" the thicker hydrocarbon regions offered by gel phases.[39]

Fluorescence Leakage *via* RF Heating. CF leakage with and without RF heating was nearly identical for DPPC liposomes, which shows that RF heating without embedded nanoparticles cannot induce leakage under the conditions employed. Furthermore, the spontaneous leakage of DPPC liposomes was considerably high after 2400 s. Without RF heating, spontaneous CF leakage decreased substantially with decreasing *L*/*N* ratio (Figure 4A, black curves). The initial leakage rate, taken as the initial slope from Figure 4A, decreased linearly with increasing nanoparticle concentration (Figure 4D), which suggests that the liposomes became more stable and yielded less spontaneous leakage with increasing nanoparticle loading. For example, at a *L*/*N* of 5000:1, the total leakage was minimal over 2400 s (3.7%) relative to DPPC. These results are consistent with DSC results and further demonstrate that nanoparticle embedment within the dML bilayers increased stability relative to DPPC liposomes.

When RF heating was applied, clear increases in the initial rates and extents of leakage from the dMLs were observed. The dMLs with a *L*/*N* ratio of 10000:1 showed the greatest initial rate and total leakage at 80% relative fluorescence intensity after 2400 s of RF heating at 250 A and 281 kHz, which yielded $Hf = 5.9 \times 10^5$ kA m^{-1} s^{-1} (Figure 4D,E). The initial rate and total leakage at *L*/*N* ratios of 25000:1 and 5000:1 were similar. On the basis of the *L*/*N* ratios examined, this indicated that an optimal nanoparticle loading was achieved for initial and total leakage at 10000:1. While an optimal loading was observed for initial and total leakage, the increase in leakage relative to no RF heating ($\%_{heating} - \%_{no\ heating}$) increased linearly with nanoparticle loading (Figure 4D).

CF release was also examined from dMLs at a *L*/*N* ratio of 10000:1 as a function of AC current from 50 to

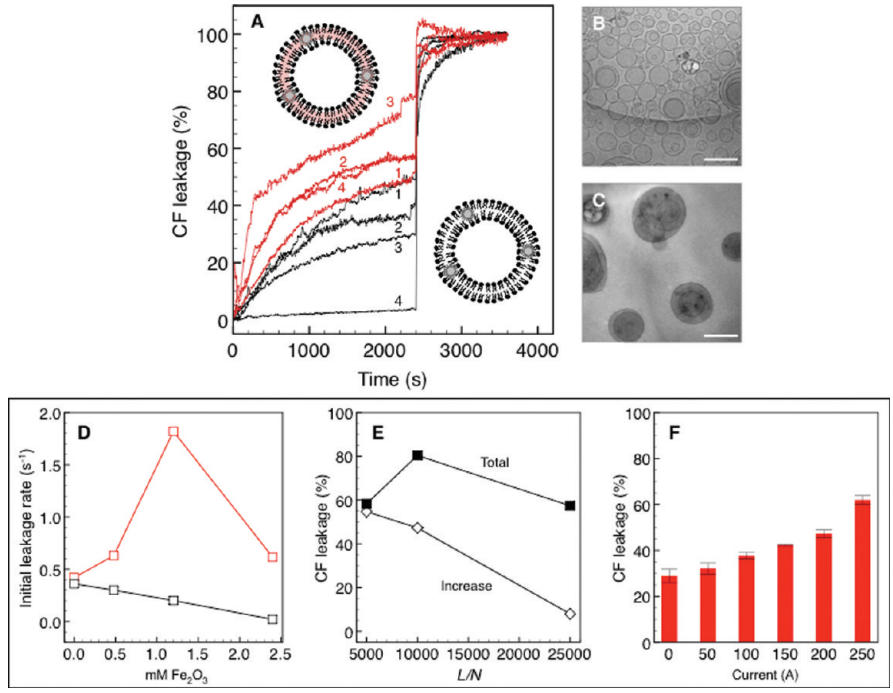

Figure 4. CF leakage from dMLs. (A) Percent CF leakage with (red) and without (black) RF heating at 250 A and 281 kHz for (1) DPPC and dMLs formed at *L/N* ratios of (2) 25000:1, (3) 10000:1, and (4) 5000:1. The inset schematics (not to scale) in (A) depict dML heating with or without RF heating. Cryo-TEM images are shown at 10 mM lipid for (B) DPPC liposomes and (C) dMLs formed at a *L/N* ratio of 10000:1 (200 nm scale bars). (D) Initial rate of leakage from (A) as a function of nanoparticle concentration with (red) and without (black) RF heating. (E) Total leakage and increase in leakage ($\%_{heating} - \%_{no\ heating}$) from (A) after 2400 s of RF heating. (F) CF leakage for dMLs at a *L/N* ratio of 10000:1 as a function of current after 2400 s of RF heating. The errors bars in (F) represent the standard deviation of duplicate experiments.

250 A, which correspond to *Hf* values from 1.0×10^5 to 5.9×10^5 kA m^{-1} s^{-1}, respectively. Increasing current led to greater total CF leakage, a 2-fold increase from 50 to 250 A, after 2400 s of RF heating (Figure 4E). Hence, the total leakage and increase in leakage in dMLs can be controlled by the extent of SPIO nanoparticle loading and the strength and duration of RF heating.

Bulk Heating Effects. The adiabatic temperature increase of samples containing ferromagnetic nanoparticles subjected to RF heating can be estimated as $dT/dt = SAR\, m_{NP} \times (c_p\, m_V)^{-1}$, where SAR is the specific absorption rate of the nanoparticles (W g^{-1}), m_{NP} is the mass of nanoparticles (g), c_p is the average heat capacity of the sample (J g^{-1} °C^{-1}, essentially that of water at dilute nanoparticle concentrations), and m_V is the mass of volume to be heated (g). To address the possible effects of bulk heating on CF leakage, calculations were performed using a SAR value of 21.5 W g^{-1}, which was measured for hydrophilic (carboxylic acid surface groups) analogues of the 5 nm SPIO nanoparticles. Temperature increases of 0.01, 0.03, and 0.06 °C were estimated for the sample after 2400 s of RF heating at 250 A and 281 kHz and nanoparticle concentrations corresponding to *L/N* ratios of 25000:1, 10000:1, and 5000:1, respectively. From ambient temperature, these increases in temperature are negligible and could not yield changes in DPPC phase behavior or permeability. Given that the system was not adiabatic, it should be noted that the calculated temperature increases represent an upper limit.

Solution temperature was monitored during RF heating experiments. In all cases, the temperature increase was approximately 6 °C and independent of SPIO nanoparticle concentration, which suggests that conductive heat transfer from the coil heated the sample. Again, this temperature increase from ambient could not alter DPPC phase behavior or permeability. Finally, to address temperature effects on CF emission intensity, measurements were performed in a dilute solution of CF in PBS from 20 to 80 °C. Only a 10.1% decrease in emission intensity was observed over this range, which confirms that bulk heating did not affect fluorescence intensity (results not shown).

Effect of RF Heating on dML Structure. Bilayer-embedded SPIO nanoparticles led to clear changes in dML structure, lipid phase behavior, and transbilayer leakage. Cryo-TEM analysis was conducted to determine if RF heating led to apparent and potentially irreversible changes in dML structure. Images of dMLs at a *L/N* ratio of 10000:1 can be seen in Figure 5, as well as in Figures 2 and 4. After being subjected to 2400 s of RF heating at 250 A and 281 kHz, partial dML fusion was observed along with the presence of bilayer sheets. The sheets were observed throughout the sample and were not found in unheated dML samples. The polygonal shape of the dMLs was due to cryogenic

preparation of the samples equilibrated at 25 °C, where the lipids were in a gel phase.[40]

Structural Features and Release Mechanisms. Nanoparticle embedment led to structural changes in the liposomes, notably the merging of neighboring bilayers. The potential role that the nanoparticles may have played in influencing bilayer structure is depicted in Figure 6. Bilayer merging observed by cryo-TEM was likely driven by the interfacial activity of the nanoparticles, the energy gain by a hydrophobic surface partitioning from water into a hydrophobic environment (bilayer),[34,41] and/or the energy penalty associated with embedding a "large defect" within a bilayer. By bridging two bilayers, neighboring (Figure 6A) or concentric liposomes (Figure 6B) appear to have fused bilayers. Both structures were observed in the cryo-TEM images (Figure 2C,D and Figure 4C), and they may account for the apparent bilayer-embedded aggregates. However, while the results support the formation of bilayer-embedded and bilayer-associated aggregates, we cannot at this time rule out the possibility that lipid-coated nanoparticles were present as encapsulated micelles.

The observation that total leakage is not proportional to nanoparticle loading may be attributed to nanoparticle aggregation within dMLs, changes in dML structure, and increased bilayer stability. Cryo-TEM analysis showed that at a *L*/*N* ratio of 5000:1 the liposomes were aggregated and contained smaller liposomes encapsulated within larger ones. This reduced the number of dMLs and the effective total surface area for leakage. The lipid phase transition was also shifted to higher temperatures, which means that more heating would be needed to surpass the phase transition temperature. In contrast, at a *L*/*N* ratio of 10000:1, the dMLs were predominantly unaggregated and yielded the greatest total leakage.

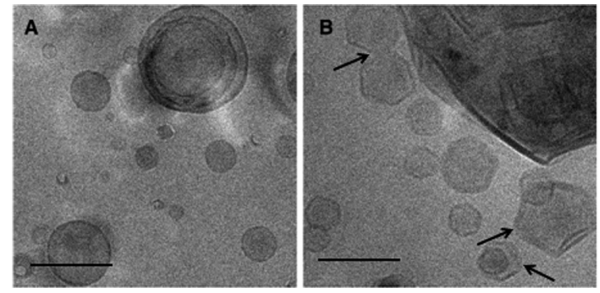

Figure 5. Cryo-TEM images of dML structure at a *L*/*N* ratio of 10000:1 (A) without and (B) with 2400 s of RF heating at 250 A and 281 kHz. The arrows in (B) denote fusion and bilayer sheets that formed after heating.

CONCLUSION

Embedding functional hydrophobic nanoparticles within lipid bilayers provides a means of controlling bilayer permeabilization and liposomal release. We have shown that 5 nm oleic acid capped SPIO nanoparticles can be embedded into DPPC bilayers to control liposomal release under physiologically acceptable EMF conditions as a function of nanoparticle loading and RF heating conditions. In turn, the ability to stabilize liposomes by nanoparticle embedment (no RF heating) provides an interesting approach to suppressing spontaneous leakage. At this stage, connections have been observed between dML structure, bilayer stability, and leakage. The presence of an optimal nanoparticle loading for controlled release depicts a trade-off between structural changes and aggregation, which reduce the effective liposome surface area, bilayer stabilization, which reduces bilayer permeability, and the localized heating in an EMF. Counterintuitively, higher nanoparticle loadings do not strictly translate into greater release. As with any therapeutic delivery system, additional experiments are needed to determine the structure, stability, and leakage characteristics of dMLs in serum and *in vivo*.

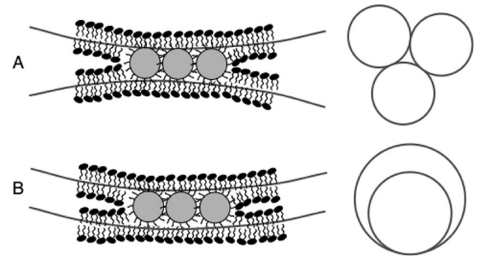

Figure 6. Proposed role of embedded SPIO nanoparticles on dML structure based on cryo-TEM analysis. Nanoparticles or nanoparticle aggregates within the bilayer led to the fusion of (A) neighboring or (B) concentric dMLs.

METHODS

Chemicals and Materials. SPIO maghemite nanoparticles (5 nm, 30 mg/mL or 187.9 mM Fe_2O_3) dispersed in chloroform were purchased from Ocean Nanotech (Springdale, AR). On the basis of the density of maghemite (4.9 g/cm^3), 30 mg/mL is equivalent to 9.4×10^{16} particles/mL. An excess or unbound oleic acid concentration of 81.5 mM was determined in the dispersions by a gas chromatograph (GC 6870, Agilent). DPPC in chloroform (20 mg/mL) was purchased from Avanti Polar Lipids (Alabaster, AL), and acetone and chloroform (>99%) were from Fisher Scientific (Suwanee, GA). 5,6-Carboxyfluorescein (CF) and Triton X-100 were purchased from Sigma Aldrich (St. Louis, MO). Phosphate buffered saline (PBS, pH 7.4) was prepared at 149 mM electrolyte concentration. Sterile deionized ultrafiltered (DI) water at 18.2 mΩ was used from a Millipore Direct-Q3 UV purification system (Billerica, MA).

dML Preparation. The dMLs were formed at 10 mM DPPC and lipid molecule to nanoparticle (*L*/*N*) ratios of 25000:1, 10000:1, and 5000:1. To prepare the samples, DPPC in chloroform (367 μL) was mixed with OA-capped SPIO nanoparticles (as received; dispersed in chloroform) in a 25 mL round-bottom flask. The volumes of the nanoparticle dispersion were 27, 67, and 135 μL for *L*/*N* ratios of 25000:1, 10000:1, and 5000:1, respectively. DI water was then added at 1 mL. Chloroform was removed by rotary evaporation at 50 °C (above the DPPC melting temperature) starting at 450 mbar for 30 min, then decreased to 300 mbar for 30 min, and finally 200 mbar for 30 min. The resulting liposomes were then bath sonicated for 1 h at 50 °C. The final sample

volume was 1 mL. For the release studies, Dulbecco's phosphate buffered saline (PBS, pH 7.4) containing 50 mM CF was used instead of DI water. CF, an anionic fluorescent dye at pH 7.4, was used as a model small molecule drug. Unencapsulated CF was removed by centrifuging the samples at 3000 rpm for 30 min, removing the supernatant by pipet, and washing with fresh PBS (repeated 3 times).

Cryogenic Transmission Electron Microscopy (Cryo-TEM). The dML samples were prepared for cryo-TEM at 25 °C using a Vitrobot (FEI Company), which is a PC-controlled robot for sample vitrification. Quantifoil grids were used with 2 μm carbon holes on 200 square mesh copper grids (Electron Microscopy Sciences, Hatfield, PA). The grid was immersed in the sample, blotted to reduce film thickness, and vitrified in liquid ethane. The sample was then transferred to liquid nitrogen for storage. Imaging was performed in a cooled stage (Model 915, Gatan Inc., Pleasonton, CA) at 200 kV using a JEOL JEM-2100F TEM (Peabody, MA). The dML size analysis was performed using ImageJ software.[42] The average size reported was based on 50 randomly selected dMLs. Energy-dispersive X-ray spectroscopy or EDS (Model INCAx-act, Oxford Instrument, UK) was used to detect elemental iron from the SPIO nanoparticles within the dMLs. EDS was conducted during cryogenic imaging with 158 s of live time and 92 s of dead time.

Differential Scanning calorimetry (DSC). Lipid phase behavior was analyzed using a TA Instruments Nano DSC (New Castle, DE). The dML samples prepared with DI water were diluted to 0.1 mM and degassed for 30 min before loading into a 0.6 mL capillary cell. The loaded samples were equilibrated at 15 °C, and sequential heat/cool cycles were performed from 15 to 50 °C at a scan rate of 1 °C min^{-1}.

Fluorescence Leakage Studies. CF leakage experiments were conducted within a fluorescence spectrometer (Model LS 55, PerkinElmer, Waltham, MA) by placing a copper heating coil (3 turns at 4.5 cm mean diameter) around a custom-designed polycarbonate cuvette holder and base. Heating was conducted as a function of time and electromagnetic field strength using a 1 kW Hotshot (Ameritherm Inc., Scottsville, NY) operating up to 250 A and 281 kHz. The samples were prepared by gently pipet mixing 5 μL of a dML sample with 2.95 mL of PBS in a quartz cuvette. Experiments were also conducted with DPPC liposomes. Once a sample was placed in the cuvette, RF heating was applied at a constant current and frequency. Triton X-100 was added after 2400 s of RF heating to solubilize the liposomes and release all CF. Fluorescence measurements were taken at excitation and emission wavelengths of 490 and 520 nm, respectively. The percent CF leakage was calculated as $100 \times [F(t) - F_0]/[F_{final} - F_0]$, where $F(t)$ was the intensity as a function of time, F_0 was the initial intensity, and F_{final} was the final intensity after the addition of Triton X-100. Experiments were conducted at room temperature (20 °C), which was below the DPPC gel to fluid main phase transition or melting temperature.

Acknowledgment. This work was supported by grants from the National Science Foundation (CBET Grants 0619440, 0828022, and 0931875) and the NASA Rhode Island Space Grant Consortium. We gratefully acknowledge M. Priess for his initial work on the RF heating system design, and Dr. R. Kingsley for his assistance with cryo-TEM analysis.

REFERENCES AND NOTES

1. Al-Jamal, W. T.; Kostarelos, K. Liposome−Nanoparticle Hybrids for Multimodal Diagnostic and Therapeutic Applications. *Nanomedicine* **2007**, *2*, 85–98.
2. Soenen, S. J. H.; Hodenius, M.; De Cuyper, M. Magnetoliposomes: Versatile Innovative Nanocolloids for Use in Biotechnology and Biomedicine. *Nanomedicine* **2009**, *4*, 177–191.
3. Weng, K. C.; Noble, C. O.; Papahadjopoulos-Sternberg, B.; Chen, F. F.; Drummond, D. C.; Kirpotin, D. B.; Wang, D. H.; Hom, Y. K.; Hann, B.; Park, J. W. Targeted Tumor Cell Internalization and Imaging of Multifunctional Quantum Dot-Conjugated Immunoliposomes *In Vitro* and *In Vivo*. *Nano Lett.* **2008**, *8*, 2851–2857.
4. Martina, M. S.; Fortin, J. P.; Menager, C.; Clement, O.; Barratt, G.; Grabielle-Madelmont, C.; Gazeau, F.; Cabuil, V.; Lesieur, S. Generation of Superparamagnetic Liposomes Revealed as Highly Efficient MRI Contrast Agents for *In Vivo* Imaging. *J. Am. Chem. Soc.* **2005**, *127*, 10676–10685.
5. Gopalakrishnan, G.; Danelon, C.; Izewska, P.; Prummer, M.; Bolinger, P. Y.; Geissbuhler, I.; Demurtas, D.; Dubochet, J.; Vogel, H. Multifunctional Lipid/Quantum Dot Hybrid Nanocontainers for Controlled Delivery of Live Cells. *Angew. Chem., Int. Ed.* **2006**, *45*, 5478–5483.
6. Bothun, G. D.; Rabideau, A. E.; Stoner, M. A. Hepatoma Cell Uptake of Cationic Multifluorescent Quantum Dot Liposomes. *J. Phys. Chem. B* **2009**, *113*, 7725–7728.
7. Al-Jamal, W. T.; Al-Jamal, K. T.; Bomans, P. H.; Frederik, P. M.; Kostarelos, K. Functionalized-Quantum-Dot-Liposome Hybrids as Multimodal Nanoparticles for Cancer. *Small* **2008**, *4*, 1406–1415.
8. Al-Jamal, W. T.; Al-Jamal, K. T.; Tian, B.; Lacerda, L.; Bomans, P. H.; Frederik, P. M.; Kostarelos, K. Lipid-Quantum Dot Bilayer Vesicles Enhance Tumor Cell Uptake and Retention *In Vitro* and *In Vivo*. *ACS Nano* **2008**, *2*, 408–418.
9. Sau, T. P.; Urban, A. S.; Dondapati, S. K.; Fedoruk, M.; Horton, M. R.; Rogach, A. L.; Stefani, F. D.; Radler, J. O.; Feldmann, J. Controlling Loading and Optical Properties of Gold Nanoparticles on Liposome Membranes. *Colloids Surf., A* **2009**, *342*, 92–96.
10. Wu, G. H.; Milkhailovsky, A.; Khant, H. A.; Fu, C.; Chiu, W.; Zasadzinski, J. A. Remotely Triggered Liposome Release by Near-Infrared Light Absorption *via* Hollow Gold Nanoshells. *J. Am. Chem. Soc.* **2008**, *130*, 8175–8177.
11. Babincova, M.; Sourivong, P.; Chorvat, D.; Babinec, P. Laser Triggered Drug Release from Magnetoliposomes. *J. Magn. Magn. Mater.* **1999**, *194*, 163–166.
12. Babincova, M.; Sourivong, P.; Leszczynska, D.; Babinec, P. Fullerenosomes: Design of a Novel Nanomaterial for Laser Controlled Topical Drug Release. *Physica Medica* **2003**, *19*, 213–216.
13. Volodkin, D. V.; Skirtach, A. G.; Mohwald, H. Near-IR Remote Release from Assemblies of Liposomes and Nanoparticles. *Angew. Chem., Int. Ed.* **2009**, *48*, 1807–1809.
14. Viroonchatapan, E.; Sato, H.; Ueno, M.; Adachi, I.; Tazawa, K.; Horikoshi, I. Release of 5-Fluorouracil from Thermosensitive Magnetoliposomes Induced by an Electromagnetic Field. *J. Controlled Release* **1997**, *46*, 263–271.
15. Babincova, M. Targeted and Controlled Release of Drugs Using Magnetoliposomes. *Ceska. Slov. Farm.* **1999**, *48*, 27–29.
16. Pradhan, P.; Giri, J.; Banerjee, R.; Bellage, J.; Bahadur, D. Preparation and Characterization of Maganese Ferrite-Based Magnetic Liposomes for Hyperthermia Treatment of Cancer. *J. Magn. Magn. Mater.* **2007**, *311*, 208–215.
17. Shinkai, M.; Yanase, M.; Honda, H.; Wakabayashi, T.; Yoshida, J.; Kobayashi, T. Intracellular Hyperthermia for Cancer Using Magnetite Cationic Liposomes: *In Vitro* Study. *Jpn. J. Cancer Res.* **1996**, *87*, 1179–1183.
18. Immordino, M. L.; Dosio, F.; Cattel, L. Stealth Liposomes: Review of the Basic Science, Rationale, and Clinical Applications, Existing and Potential. *Int. J. Nanomed.* **2006**, *1*, 297–315.
19. De Cuyper, M.; Joniau, M. Magnetoliposomes: Formation and Structural Characterization. *Eur. Biophys. J.* **1988**, *15*, 311–319.
20. Wijaya, A.; Hamad-Schifferli, K. High Density Encapsulation of Fe_3O_4 Nanoparticles in Lipid Vesicles. *Langmuir* **2007**, *23*, 9546–9550.
21. Zhang, J. Q.; Zhang, Z. R.; Yang, H.; Tan, Q. Y.; Qin, S. R.; Qiu, X. L. Lyophilized Paclitaxel Magnetoliposomes as a Potential Drug Delivery System for Breast Carcinoma *via* Parenteral Administration: *In Vitro* and *In Vivo* Studies. *Pharm. Res.* **2005**, *22*, 573–583.
22. Mornet, S.; Vasseur, S.; Grasset, F.; Duguet, E. Magnetic Nanoparticle Design for Medical Diagnosis and Therapy. *J. Mater. Chem.* **2004**, *14*, 2161–2175.
23. Pankhurst, Q. A.; Connolly, J.; Jones, S. K.; Dobson, J.

Applications of Magnetic Nanoparticles in Biomedicine. *J. Phys. D* **2003**, *36*, 167–181.
24. Saiyed, Z.; Telang, S.; Ramchand, C. Application of Magnetic Techniques in the Field of Drug Discovery and Biomedicine. *Biomagn. Res. Technol.* **2003**, *1*, 2.
25. Tartaj, P.; Morales, M.; Verdaguer, S. V.; Carreno, T. G. ; Serna, C. J. The Preparation of Magnetic Nanoparticles for Applications in Biomedicine. *J. Phys. D* **2003**, *36*, 182–197.
26. Duguet, E.; Vasseur, S.; Mornet, S.; Devoisselle, J. M. Magnetic Nanoparticles and Their Applications in Medicine. *Nanomedicine* **2006**, *1*, 157–168.
27. Brezovich, I. A. Low Frequency Hyperthermia. *Med. Phys. Monograph* **1988**, *16*, 82–111.
28. Chen, Y. J.; Bothun, G. D. Lipid-Assisted Formation and Dispersion of Aqueous and Bilayer-Embedded Nano-C_{60}. *Langmuir* **2009**, *25*, 4875–4879.
29. Jeng, U.-S.; Hsu, C.-H.; Lin, T.-L.; Wu, C.-M.; Chen, H.-L.; Tai, L.-A.; Hwang, K.-C. Dispersion of Fullerenes in Phospholipid Bilayers and the Subsequent Changes in the Host Bilayers. *Physica B* **2005**, *357*, 193–198.
30. Binder, W. H.; Sachsenhofer, R.; Farnik, D.; Blaas, D. Guiding the Location of Nanoparticles into Vesicular Structures: A Morphological Study. *Phys. Chem. Chem. Phys.* **2007**, *9*, 6435–6441.
31. Park, S.-H.; Oh, S.-G.; Mun, J.-Y.; Han, S.-S. Loading of Gold Nanoparticles inside the DPPC Bilayers of Liposome and Their Effects on Membrane Fluidities. *Colloids Surf., B* **2006**, *48*, 112–118.
32. Bothun, G. D. Hydrophobic Silver Nanoparticles Trapped in Dipalmitoylphosphatidylcholine Bilayers: Size Distribution, Bilayer Phase Behavior, and Optical Properties. *J. Nanobiotechnology* **2008**, DOI: 10.1186/1477-3155-6-13.
33. Park, S. H.; Oh, S. G.; Mun, J. Y.; Han, S. S. Effects of Silver Nanoparticles on the Fluidity of Bilayer in Phospholipid Liposome. *Colloids Surf., B* **2005**, *44*, 117–22.
34. Jang, H.; Pell, L. E.; Korgel, B. A.; English, D. S. Photoluminescence Quenching of Silicon Nanoparticles in Phospholipid Vesicle Bilayers. *J. Photochem. Photobiol. A* **2003**, *158*, 111–117.
35. Binder, W. H.; Sachsenhofer, R. Polymersome/Silica Capsules by 'Click'-Chemistry. *Macromol. Rapid Commun.* **2008**, *29*, 1097–1103.
36. Mueller, W.; Koynov, K.; Fischer, K.; Hartmann, S.; Pierrat, S.; Basche, T.; Maskos, M. Hydrophobic Shell Loading of PB-*b*-PEO Vesicles. *Macromolecules* **2009**, *42*, 357–361.
37. Nagle, J. F.; Tristram-Nagle, S. Structure of Lipid Bilayers. *Biochim. Biophys. Acta* **2000**, *1469*, 159–195.
38. Inoue, T.; Yanagihara, S.; Misono, Y.; Suzuki, M. Effects of Fatty Acids on Phase Behavior of Hydrated Dipalmitoylphosphatidylcholine Bilayer: Saturated *versus* Unsaturated Fatty Acids. *Chem. Phys. Lipids* **2001**, *109*, 117–133.
39. Ivanova, V. P.; Heimburg, T. Histogram Method to Obtain Heat Capacities in Lipid Monolayers, Curved Bilayers, and Membranes Containing Peptides. *Phys. Rev. E* **2001**, *63*, 1914–1925.
40. Frederik, P. M.; Stuart, M. C. A.; Bomans, P. H. H.; Lasic, D. D. Cryo-Electron Microscopy of Liposomes. In *Nonmedical Applications of Liposomes, Theory and Basic Sciences*; Lasic, D. D., Barenholz, Y., Eds.; CRC Press: Boca Raton, FL, 1996; pp 309−322.
41. Wi, H. S.; Lee, K.; Pak, H. K. Interfacial Energy Consideration in the Organization of a Quantum Dot−Lipid Mixed System. *J. Phys.: Condens. Mater.* **2008**, *20*, 1–6.
42. Abramoff, M. D.; Magelhaes, P. J.; Ram, S. J. Image Processing with ImageJ. *Biophotonics Int.* **2004**, *11*, 36–42.